

# Structure of MCM-48 Revealed by Transmission Electron Microscopy

Viveka Alfredsson and Michael W. Anderson\*

Department of Chemistry, UMIST, P.O. Box 88, Manchester M60 1QD, U.K.

Received December 4, 1995. Revised Manuscript Received February 22, 1996<sup>Ⓢ</sup>

A model of the cubic mesoporous silicate MCM-48, based on the gyroid minimal surface, has been generated by computer simulation. Transmission electron micrographs and X-ray diffraction (XRD) patterns have been recorded for MCM-48 and compared with the images and XRD patterns obtained by modeling. The gyroid minimal surface gives an excellent description for the structure of MCM-48 with the amorphous hydroxylated silicate sited close to the midplane of the surface.

## Introduction

With the synthesis of the silica-based M41S, first reported in 1992,<sup>1</sup> a new class of porous material was discovered. These materials contain large, uniform cages and channels in the mesopore size regime (15–100 Å). Despite the regularity of the channel systems the wall structure of M41S materials are essentially amorphous. The first structures to be reported were the hexagonal (MCM-41), lamellar (MCM-50), and cubic (MCM-48) phases<sup>2</sup> but other structures have since been synthesized.<sup>3,4</sup> Within these structure types the chemical composition of the walls has also been modified greatly.<sup>5</sup> The synthesis proceeds via a hydrothermal reaction of, generally, a siliceous gel mixed with a surfactant, typically cetyltrimethylammonium chloride (CTACl), which acts in some manner as a template.

The hexagonal phase (MCM-41) has so far been the most intensely studied member of these mesoporous materials although its structure is not as well defined from a crystallographic point of view as that of its cubic counterpart, MCM-48. MCM-41 has been described as being built from hexagonally arranged tubes, with diameters ranging from ca. 20 to 100 Å depending on the type of surfactant used in the synthesis. These tubes are generally not straight but wind as might a bunch of ropes. The structure viewed by electron microscopy in the direction along the tubes (in a narrow section where the tubes are essentially straight) resembles an image of a honeycomb net. MCM-48 on the

other hand has a cubic structure with space group  $Ia\bar{3}d$ .<sup>1</sup> The structure has been “conjectured” to coincide with that of a minimal surface.<sup>6</sup>

To define a minimal surface, the concept of the principal curvatures needs to be introduced. Consider the normal vector at a point on the surface. A plane containing the vector intersects the surface in a plane curve which has a certain curvature. If this plane is allowed to rotate around the normal vector, an infinite number of planes with continuously varying curvatures at the intersection with the point on the surface is obtained. The largest and the smallest value of these different curvatures are called the principal curvatures,  $c_1$  and  $c_2$ . For a surface to be a minimal surface, the principal curvatures must be equal in magnitude but opposite in sign. This means that the mean curvature,  $H = 1/2(c_1 + c_2)$ , of the surface is zero. The Gaussian curvature, defined as  $K = c_1 c_2$ , is either negative or, at the so-called flat points, zero. This implies that the surface is as concave as it is convex, except at the flat points. For a more detailed and mathematical description see the works of Andersson et al.<sup>7,8</sup>

If the surface exhibits crystallographic periodicity, it is called an infinite periodic minimal surface (IPMS). Such surfaces have been successfully used not only for describing crystalline solids,<sup>7,8</sup> such as for example the structure of the zeolites A, N, and Y, but also in lipid–water<sup>9–11</sup> systems.

There are several cubic IPMS (e.g., the P, the D, and the gyroid surface). Examples of structures that are described by these surfaces are zeolite A (LTA) which

<sup>Ⓢ</sup> Abstract published in *Advance ACS Abstracts*, April 1, 1996.

(1) Kresge, C. T.; Leonowicz, M. E.; Roth, W. J.; Vartuli, J. C.; Beck, J. S. *Nature* **1992**, *359*, 710.

(2) Beck, J. S.; Vartuli, J. C.; Roth, W. J.; Leonowicz, M. E.; Kresge, C. T.; Schmitt, K. D.; Chu, C. T.-W.; Olson, D. H.; Sheppard, E. W.; McCullen, S. B.; Higgins, J. B.; Schenker, J. L. *J. Am. Chem. Soc.* **1992**, *114*, 10835.

(3) Huo, Q.; Margolese, D. I.; Ciesla, U.; Demuth, D. G.; Feng, P.; Gier, T. E.; Sieger, P.; Firouzi, A.; Chmelka, B. F.; Schüth, F.; Stucky, G. D. *Chem. Mater.* **1994**, *6*, 1176.

(4) Huo, Q.; Leon, R.; Petroff, P. M.; Stucky, G. D. *Science* **1995**, *268*, 1324.

(5) Huo, Q.; Margolese, D. I.; Ciesla, U.; Feng, P.; Gier, T. E.; Sieger, P.; Leon, R.; Petroff, P. M.; Schüth, F.; Stucky, G. D. *Nature* **1994**, *368*, 317.

(6) Monnier, A.; Schüth, F.; Huo, Q.; Kumar, D.; Margolese, D.; Maxwell, R. S.; Stucky, G. D.; Krishnamurty, M.; Petroff, P.; Firouzi, A.; Janicke, M.; Chmelka, B. F. *Science* **1993**, *261*, 1299.

(7) Andersson, S.; Hyde, S. T.; von Schnering, H.-G. *Z. Kristall.* **1984**, *168*, 1.

(8) Andersson, S.; Hyde, S. T.; Larsson, K.; Lidin, S. *Chem. Rev.* **1988**, *88*, 221.

(9) Larsson, K.; Fontell, K.; Krog, N. *Chem. Phys. Lipids* **1980**, *27*, 321.

(10) Hyde, S. T.; Andersson, S.; Ericsson, B.; Larsson, K. *Z. Kristall.* **1984**, *168*, 213.

(11) Larsson, K. *J. Phys. Chem.* **1989**, *93*, 7304.

(12) Schoen, A. H. NASA Technical Note D-5541, Washington, D. C. 1970.

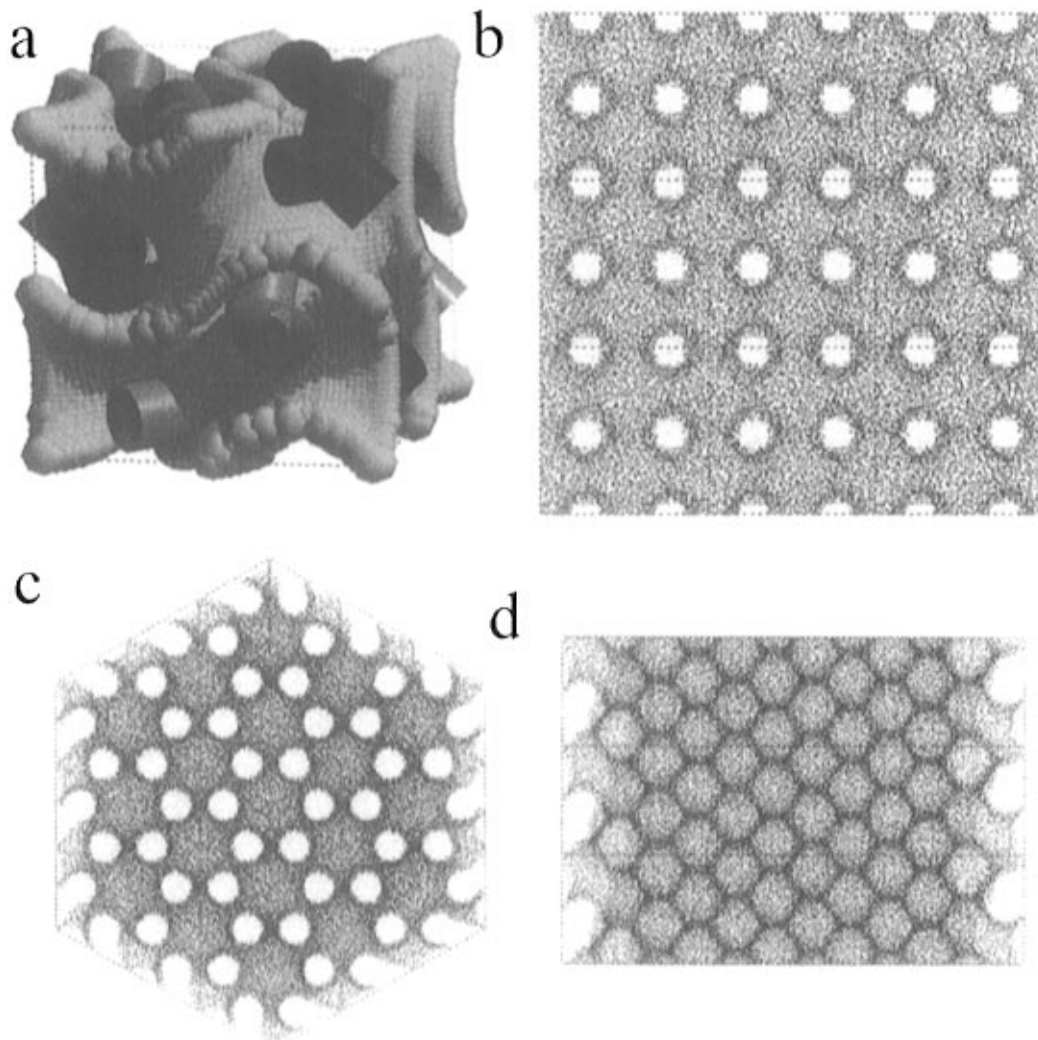


**Figure 1.** Representation of the gyroid minimal surface: (a) the gyroid minimal surface in light gray with the two interweaving rods (dark gray and black) of the  $Q^{230}$  structure. It is believed that during synthesis the surfactant forms the  $Q^{230}$  rod structure and the silicate condenses in between along the gyroid minimal surface; (b) an example of the [100] projection generated for TEM and XRD simulations of MCM-48 consisting only of silicon atoms randomly dispersed around the gyroid surface with an average separation of 3.03 Å and a wall thickness of ca. 6 Å; (c) the projection along [111]; (d) the projection along [110]. Along [100] and [111] there are channels running through the structure whereas in the [110] direction the channel like appearance obtained in TEM micrographs is created by the large electron density difference in projection in different regions.

can be fitted to one side of the P surface<sup>7</sup> and faujasite (FAU) which can be fitted to one side of the D surface (sometimes referred to as the F surface).<sup>7</sup> The gyroid or G surface was discovered by Schoen in 1970.<sup>13</sup>

The gyroid is perhaps the most complex of the three fundamental cubic IPMS. It partitions space into two equal but nonintersecting compartments, which means that two molecules on each side of the surface will never meet. The space group is  $Ia\bar{3}d$  and the surface is the result of sine waves oscillating in three dimensions. It has been shown that the gyroid can be approximated by the following simple analytical function:<sup>13</sup>

$$\cos x \sin y + \cos y \sin z + \sin x \cos z = 0 \quad (1)$$

See Figure 1a. The two 3-dimensional channel systems which are created on either side of the gyroid surface form an enantiomorphic pair. The channel systems are

represented by the intertwined rods also shown in Figure 1a (known as the  $Q^{230}$  rod model<sup>14</sup>). The gyroid surface in projection adopts a variety of interesting patterns. For instance, along [100] and [111] (Figure 1b,c) uninterrupted channels are observed but along other principle directions, such as [110] (Figure 1d), no channels are observed. However, owing to changes in curvature, the density of the surface in projection varies considerably. This is manifested as a variety of regular patterns.

MCM-48 has been described by Monnier et al.<sup>6</sup> to have a remarkable similarity with the  $Ia\bar{3}d$  phase found in the water-CTABr system,<sup>15</sup> which agrees very well with the  $Q^{230}$  model, first described as a rod structure<sup>14</sup> and later realized also to be related to that of the gyroid minimal surface,<sup>10,16</sup> with the solvated surfactant head-

(13) von Schnering, H. G.; Nesper, R. *Z. Phys. B-Condens. Mater.* **1991**, 407.

(14) Luzzati, V.; Speg, P. A. *Nature* **1967**, 215, 701.

(15) Auvray, X.; Petipas, C.; Anthore, R.; Rico, I.; Lattes, A. *J. Phys. Chem.* **1989**, 93, 7458.

(16) Mariani, P.; Luzzati, V.; Delacroix, H. *J. Mol. Biol.* **1988**, 204, 165.

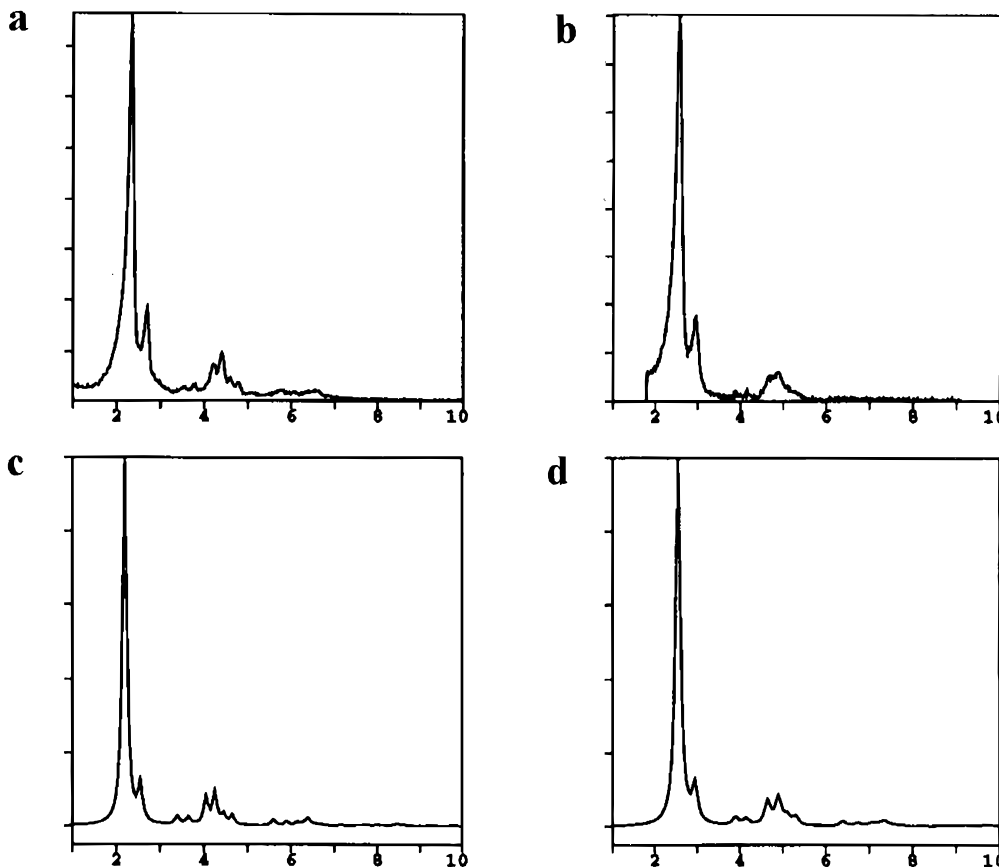


**Figure 2.** XRD pattern of (a) uncalcined MCM-48, and (b) calcined MCM-48, simulated pattern from the structure shown in Figure 1b for a unit cell of 97.3 Å (c) and 85 Å (d). The simulations were made for a particle size of  $750 \times 750 \times 750$  Å. To obtain a better match between the XRD between the calcined sample and its corresponding simulated pattern, a small (0.5%) lattice strain was used in the calculation.

groups meeting near the minimal surface and the tails filling the rod structure. The water layer forms the gyroid surface. For MCM-48 the structure has been suggested to be equivalent<sup>6</sup> with the midplane of the silicate walls sited on the minimal surface and the head of the surfactant bound to the silicate. The conclusions drawn by Monnier et al.<sup>6</sup> were based on the fact that the XRD pattern of MCM-48 agrees very well with the calculated XRD pattern using a model based on the  $Q^{230}$  structure. However, the lack of phase information in a diffraction pattern means that the structure cannot be unambiguously determined. In a paper by Schmidt et al.<sup>17</sup> the space group of MCM-48 was confirmed. This conclusion was drawn from the fact that the optical diffraction pattern from TEM images as well as the XRD pattern fit with the space group  $Ia\bar{3}d$ . In this work we show that the structure of MCM-48 does indeed fit very well with the gyroid minimal surface as evidenced from a comparison of experimental transmission electron micrographs (where phase information is retained) with simulations based on the gyroid surface. Furthermore, the simulated structure accounts for the intensity of all reflections in both electron and x-ray diffraction patterns.

### Experimental Section

**Synthesis.** The following chemicals were used in the synthesis: tetraethylorthosilicate (TEOS) 98% solution from Aldrich; cetyltrimethylammonium chloride (CTACl) 25% from Aldrich; NaOH from BDH. MCM-48 was synthesized in accordance with the molar ratio given in reference 6 (1 mol of TEOS:0.25 mol of  $Na_2O$ :0.65 mol of CTACl:62 mol of  $H_2O$ ). The reactants were stirred to a homogeneous gel and heated to 95 °C for 4 days. The product which is a white powder was filtered and washed with distilled water. The XRD pattern, shown in Figure 2a, is the same as that previously reported for MCM-48 with a unit cell of 97.3 Å. The sample was subsequently calcined at 300 °C. This treatment leaves a slightly discolored powder indicating that the surfactant has not been quantitatively removed. However, in the XRD pattern, shown in Figure 2b, the peaks of MCM-48 can be observed, although slightly less sharp than for the uncalcined sample and with the cell parameter reduced to approximately 85 Å.

**Transmission Electron Microscopy.** The specimens were dispersed in acetone and placed on holey carbon grids. Two transmission microscopes were used, Philips 430 (300 kV, Cs = 2.0 mm) and Philips CM200 (200 kV, Cs = 2.0 mm). As the stability of the specimen is affected by the electron beam and rapidly disintegrates, the images were recorded at relatively low magnifications in order to diminish the deteriorating effect of the beam. Both the uncalcined and the calcined sample were imaged. The stability of the specimen in the microscope is noticeably enhanced after calcination. Higher accelerating voltage, 300 kV as opposed to 200 kV, also gives

(17) Schmidt, R.; Stöcker, M.; Akporiaye, D.; Heggelund Törstad, E.; Olsen, A. *Micropor. Mater.* **1995**, *5*, 1.

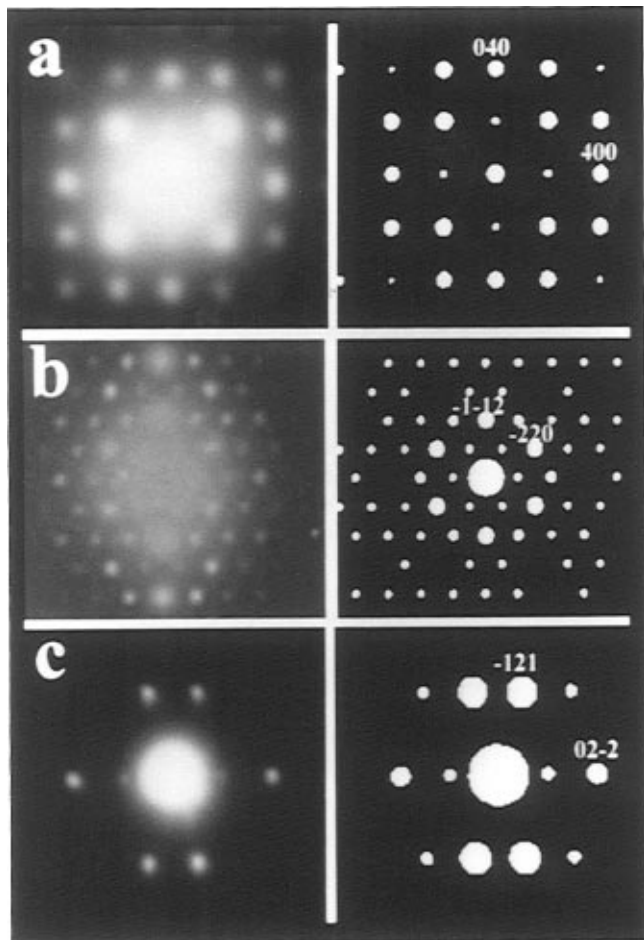


**Figure 3.** Selected area electron diffraction patterns (left) and simulations (right) for MCM-48 along [001] (a), along [111] (b), and along [311] (c).

a significant improvement in the stability of the specimen to the electron beam.

**Computer Simulations.** To simulate atomic positions near the gyroid surface a simple Fortran program was used. The unit cell ( $a = 97.3 \text{ \AA}$ ) was divided into small cubes with edges of  $3.03 \text{ \AA}$  (the average separation between Si atoms in a silicate material). At each cube vertex the analytical equation (eq 1) of the gyroid surface was tested. If the absolute value of the equation was smaller than a specified value, a Si atom was inserted in that position (only Si atoms were used in the calculations). To remove the gridlike appearance thus obtained, all the atoms were displaced by a small random value from their original position but with their average separation retained. This created a minimal surface with an amorphous-like wall with a thickness of about  $6 \text{ \AA}$ . For the simulations of the calcined MCM-48 the unit cell parameter was reduced to  $85 \text{ \AA}$ . The unit cell contained 6280 atoms.

The XRD pattern, the selected area electron diffraction (SAED) pattern, and the TEM image simulations were calculated with Cerius<sup>2</sup>. The XRD pattern was calculated for a crystallite size of  $750 \times 750 \times 750 \text{ \AA}$ , which corresponds to the actual size of the synthetic particles, for Cu K $\alpha$  radiation. The TEM images were simulated with the following parameters: accelerating voltage  $300 \text{ kV}$ , spherical aberration constant  $2.0 \text{ mm}$ , defocus spread  $150 \text{ \AA}$ , and beam spread  $3.5 \text{ mrad}$ . The unit cell was sliced with a slice thickness on the order of  $1\text{--}2 \text{ \AA}$  depending on the direction of the respective images. The images for Figure 5 were calculated for the smallest repeat distance in the respective direction. However, the appearance of the images varies only slightly with thick-

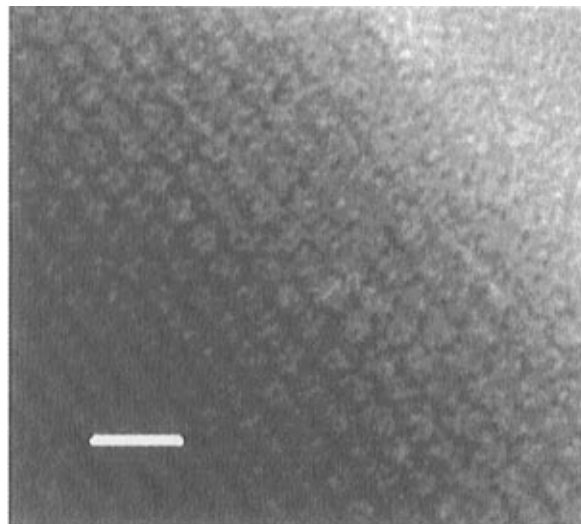


**Figure 4.** Transmission electron micrograph of the uncalcined MCM-48 along [110] recorded at  $200 \text{ kV}$ . Scale bar:  $97 \text{ \AA}$ .

ness, and determining the thickness of the respective particles by comparison with the simulated images was not possible.

**Image Processing.** Image processing was performed with the Semper image-processing system. Experimental micrographs were read by a slow-scan CCD camera. The Fourier transform of the images was calculated and the lattice indexed. Lattice parameters were determined from the strongest peaks in the transform. These peaks retain both amplitude and phase information. The intensity of the signal is estimated via the integrated intensity in a  $2 \times 2$  pixel region, with the local background subtracted, and the phase is given by the average of the phase in these points. Only this information is used for calculating the averaged image via a reverse Fourier transform.<sup>18,19</sup>

## Results

Simulations of XRD patterns, electron micrographs, and electron diffraction patterns using the model of MCM-48 based on the gyroid minimal surface, clearly demonstrate how well this model represents the actual structure of MCM-48. Figure 2 shows the experimentally obtained XRD pattern of the uncalcined sample (2a) and of the calcined sample (2b) together with those calculated from the gyroid model for a unit cell of  $97.3 \text{ \AA}$  (2c) and  $85 \text{ \AA}$  (2d). The latter was simulated with a small amount of strain ( $0.5\%$ ) in the structure. As can be seen, the fit is very good with all reflections occurring, with correct intensities. Figure 3 shows similar comparisons for the electron diffraction patterns along three directions.

The gyroid was calculated for different thicknesses of the surface, and a surface with an approximate thickness of  $6 \text{ \AA}$  was used in the image simulations and in the XRD pattern simulation. However, the surface thickness does not significantly alter the resulting simulated images. The electron microscope images were simulated for low underfocus values as the micrographs

(18) Carlsson, A. *Electron Microsc.* **1**, EUREM 92, Granada, Spain, 497, 1992.

(19) Hovmöller, S.; Sjögren, A.; Farrants, G.; Sundberg, M.; Marinder, B.-O. *Nature* **1984**, *311*, 238.

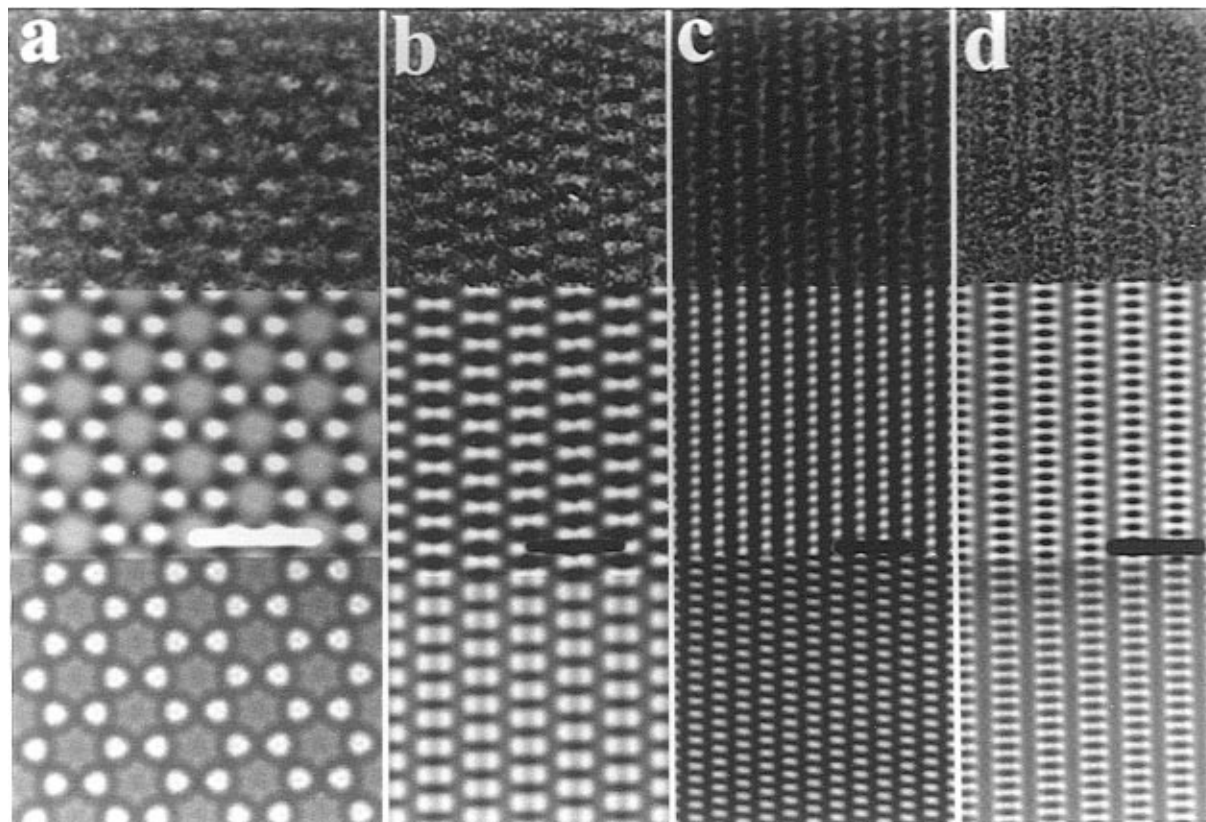


**Figure 5.** Transmission electron micrographs of the calcined MCM-48 ( $a = 85 \text{ \AA}$ ) along different directions (top row), the same images after image processing (middle row) and the corresponding simulated images (bottom row): (a) along [111] (scale bar  $120 \text{ \AA}$ ); (b) along [311] (scale bar  $63 \text{ \AA}$ ); (c) along [432] (scale bar  $105 \text{ \AA}$ ); (d) along [335] (scale bar  $122 \text{ \AA}$ ). The simulated images were calculated using the following parameters: (a) focus  $-2000 \text{ \AA}$ , slice thickness  $1.47 \text{ \AA}$ , total thickness  $147 \text{ \AA}$ ; (b) focus  $-2000 \text{ \AA}$ , slice thickness  $1.4 \text{ \AA}$ , total thickness  $281 \text{ \AA}$ ; (c) focus  $-2000 \text{ \AA}$ , slice thickness  $1.83 \text{ \AA}$ , total thickness  $458 \text{ \AA}$ ; (d) focus  $-2000 \text{ \AA}$ , slice thickness  $1.11 \text{ \AA}$ , total thickness  $557 \text{ \AA}$ .

were recorded under such conditions. As all the reflections for MCM-48 occur at small scattering vectors—the unit cell being very large—there is no need to record images at Scherzer focus which is generally the optimum focus for high-resolution imaging. At Scherzer focus the largest number of reflections are given the right phase. When the focus is lowered (within certain limits) the transfer for reflections with small scattering vectors, that is reflections that represent crystal planes with large interplane distances such as those occurring in MCM-type of materials, is enhanced but reflections with larger scattering vectors are given opposite contrast. However, as the only reflections that occur in MCM-48 are at small scattering vectors, as there is no short-range order in this type of material, a lower focus is preferential.

Electron micrographs have been recorded along several different directions, [111], [110], [311], [432], and [335] (the [111] direction image is similar to that reported previously by Monnier et al.<sup>6</sup> and Vartuli et al.,<sup>20</sup> whereas Schmidt et al.<sup>17</sup> reported several different directions). The incident beam directions of the micrographs were determined either from the corresponding SAED patterns or from the optical diffractograms of the

micrograph, obtained via the Semper software. Figure 4 shows a micrograph, recorded along [110], of the uncalcined sample of MCM-48. This direction is well matched by the simulated micrographs (not shown). The other micrographs (shown in Figure 5) are all from the calcined sample as this was more stable in the microscope and easier to image. To improve the quality of the images the micrographs (top images in Figure 5) were processed and the average images calculated (center images in Figure 5). These images were then compared with the images simulated for the model described above (bottom images in Figure 5) and, as can be seen, the agreement between MCM-48 and the gyroid model is excellent. It should be noted that the variation in contrast in these images is not due to pores running through the material in projection. The contrast variation is due only to changes in electron density of the wall in projection, i.e., a wall with plane perpendicular to the beam direction represents a low electron density in projection and a wall with plane parallel to the beam direction represents a high electron density in projection. In the images shown only the [111] direction exhibits pores in projection (see Figure 1b). The [100] direction (not shown) would also have pores in projection.

Figure 6 shows the effect of wall thickness on the simulated TEM images of MCM-48. Simulations were made for wall thicknesses between  $3$  and  $13 \text{ \AA}$ . Small

(20) Vartuli, J. C.; Schmitt, K. D.; Kresge, C. T.; Roth, W. J.; Leonowicz, M. E.; McCullen, S. B.; Hellring, S. D.; Beck, J. S.; Schlenker, J. L.; Olson, D. H.; Sheppard, E. W. *Chem. Mater.* **1994**, *6*, 2317.

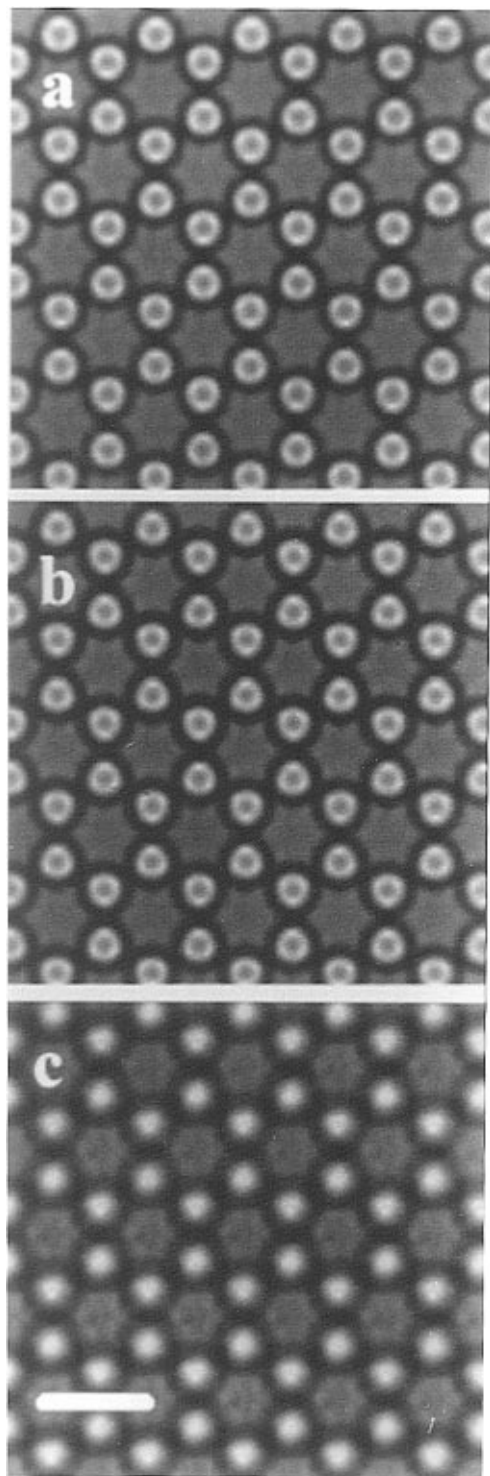


**Figure 6.** Simulated transmission electron micrographs of MCM-48 along the [111] direction showing the effect of wall thickness. The thicknesses used were approximately (a) 3 Å, (b) 6 Å, and (c) 13 Å. The following parameters were used for the simulations: focus -1500 Å, slice thickness 1.68 Å, total thickness 84 Å.

changes are clearly observable between these images; however, we do not feel confident about using such a technique to accurately determine wall thicknesses in MCM-48. The accuracy of wall thickness calculations is probably no better than *ca.*  $\pm 5$  Å assuming the wall thickness to be constant. This is highly unlikely in an essentially amorphous material.

### Discussion

We have shown that the structure of MCM-48 does indeed fit to the gyroid minimal surface as was previously conjectured by Monnier et al.<sup>6</sup> The previous report relied on the XRD pattern. In this work, by simulation of an amorphous silicate network based around the gyroid surface and simulation of TEM micrographs as well as XRD patterns, it has been possible to confirm these previous suggestions. The results rule out the possibility, for instance, that the silicate walls of the MCM-48 structure follows the  $Q^{230}$  rod model of Luzzati et al.<sup>15</sup> However, it is quite probable that the surfactant molecules form the  $Q^{230}$  rod structure during synthesis with the silicate walls condensing between the rods along the gyroid minimal surface as proposed by Monnier et al.<sup>6</sup> The simulated XRD pattern obtained from the model described above fits very well with the experimentally obtained pattern. Also, all the diffraction patterns and the optical diffraction patterns obtained from micrographs recorded of the samples could be indexed according to space group 230 ( $Ia\bar{3}d$ ). Furthermore, the images, recorded along various directions, could be matched with the corresponding images simulated for the gyroid. MCM-48 is a beautiful example of how matter forms according to an IPMS and, to our knowledge, represents the first synthetic material, which continuously follows such a surface, which has been directly imaged. Natural materials such as the single calcite crystals in platelets of sea urchins have been recognized to lie on the P surface.<sup>21</sup> This proof that the midplane of MCM-48 lies on the gyroid minimal surface, as originally suggested in ref 6, is also indirect supportive evidence that the  $Ia\bar{3}d$  liquid-crystalline mesophase is a bicontinuous structure based on the gyroid surface as proposed by Mariani et al.<sup>16</sup>

**Acknowledgment.** The authors thank the Swedish Research Council for Engineering Sciences for financial support to V.A. and EPSRC for support for M.W.A. The authors would also like to thank Donat-Pierre Luigi for assistance with computer programming and Stephen T. Hyde for useful discussions on minimal surfaces.

CM950568K

(21) Donnay, G.; Pawson, D. L. *Science* **1969**, *166*, 1147.